Biomedical Optics EXPRESS

Temperature-sensitive gating of hCx26: high-resolution Raman spectroscopy sheds light on conformational changes

Ann-Kathrin Kniggendorf,[1,*] Merve Meinhardt-Wollweber,[1,2] Xiaogang Yuan,[1] Bernhard Roth,[1] Astrid Seifert,[3] Niels Fertig,[3] and Carsten Zeilinger[4,5]

[1]*Hanover Centre for Optical Technologies, Gottfried-Wilhelm-Leibniz Universität Hannover, Nienburger Str. 17, 30167 Hanover, Germany*
[2]*Cluster of Excellence Hearing4All, Hanover, Germany*
[3]*Nanion Technologies GmbH, Gabrielenstr. 9, 80636 Munich, Germany*
[4]*Gottfried-Wilhelm-Leibniz Universität Hannover and Biomolekulares Wirkstoffzentrum, Herrenhäuser Str. 2, 30419 Hanover, Germany*
[5]*zeilinger@biophysik.uni-hannover.de*
[*]*ann.kathrin.kniggendorf@hot.uni-hannover.de*

Abstract: The temperature-sensitive gating of human Connexin 26 (hCx26) was analyzed with confocal Raman microscopy. High-resolution Raman spectra covering the spectral range between 400 and 1500 rel. cm^{-1} with a spectral resolution of 1 cm^{-1} were fully annotated, revealing notable differences between the spectrum recorded from solubilized hCx26 in Ca^{2+}-buffered POPC at 10°C and any other set of protein conditions (temperature, Ca^{2+} presence, POPC presence). Spectral components originating from specific amino acids show that the TM1/EL1 parahelix and probably the TM4 trans-membrane helix and the plug domain are involved in the gating process responsible for fully closing the hemichannel.

OCIS codes: (180.5655) Raman microscopy; (170.1420) Biology.

References and links

1. C. Peracchia, "Chemical gating of gap junction channels; roles of calcium, pH and calmodulin," Biochim. Biophys. Acta **1662**(1-2), 61–80 (2004).
2. F. F. Bukauskas and V. K. Verselis, "Gap junction channel gating," Biochim. Biophys. Acta **1662**(1-2), 42–60 (2004).
3. T. A. Bargiello, Q. Tang, S. Oh, and T. Kwon, "Voltage-dependent conformational changes in connexin channels," Biochim. Biophys. Acta **1818**(8), 1807–1822 (2012).
4. M. Steffens, F. Göpel, A. Ngezahayo, C. Zeilinger, A. Ernst, and H. A. Kolb, "Regulation of connexons composed of human connexin26 (hCx26) by temperature," Biochim. Biophys. Acta **1778**(5), 1206–1212 (2008).
5. G. M. Hand, D. J. Müller, B. J. Nicholson, A. Engel, and G. E. Sosinsky, "Isolation and characterization of gap junctions from tissue culture cells," J. Mol. Biol. **315**(4), 587–600 (2002).
6. S. Maeda, S. Nakagawa, M. Suga, E. Yamashita, A. Oshima, Y. Fujiyoshi, and T. Tsukihara, "Structure of the connexin 26 gap junction channel at 3.5 A resolution," Nature **458**(7238), 597–602 (2009).
7. C. Ambrosi, D. Boassa, J. Pranskevich, A. Smock, A. Oshima, J. Xu, B. J. Nicholson, and G. E. Sosinsky, "Analysis of four connexin26 mutant gap junctions and hemichannels reveals variations in hexamer stability," Biophys. J. **98**(9), 1809–1819 (2010).
8. S. A. Oladepo, K. Xiong, Z. Hong, and S. A. Asher, "Elucidating Peptide and Protein Structure and Dynamics: UV Resonance Raman Spectroscopy," J. Phys. Chem. Lett. **2**(4), 334–344 (2011).
9. I. H. McColl, E. W. Blanch, A. C. Gill, A. G. Rhie, M. A. Ritchie, L. Hecht, K. Nielsen, and L. D. Barron, "A New Perspective on β-Sheet Structures Using Vibrational Raman Optical Activity: From Poly(L-lysine) to the Prion Protein," J. Am. Chem. Soc. **125**(33), 10019–10026 (2003).
10. C. Zeilinger, M. Steffens, and H. A. Kolb, "Length of C-terminus of rCx46 influences oligomerization and hemichannel properties," Biochim. Biophys. Acta **1720**(1-2), 35–43 (2005).
11. A. Kniggendorf, T. Gaul, and M. Meinhardt-Wollweber, "Hierarchical Cluster Analysis (HCA) of Microorganisms: An Assessment of Algorithms for Resonance Raman Spectra," Appl. Spectrosc. **65**(2), 165–173 (2011).
12. A. Rygula, K. Majzner, K. M. Marzec, A. Kaczor, M. Pilarczyk, and M. Baranska, "Raman spectroscopy of proteins: a review," J. Raman Spectrosc. **44**(8), 1061–1076 (2013).
13. D. Němeček and G. J. Thomas, Jr., "Raman Spectroscopy of Viruses and Viral Proteins," in *Frontiers of Molecular Spectroscopy*, J. Laane, ed. (Elsevier, 2009).

#207404 - $15.00 USD Received 28 Feb 2014; revised 5 May 2014; accepted 5 May 2014; published 6 Jun 2014

14. F. S. Parker, *Biochemistry*, (Plenum Press, New York, 1983).
15. M. C. Chen and R. C. Lord, "Laser-Excited Raman Spectroscopy of Biomolecules. VI. Some Polypeptides as Conformational Models," J. Am. Chem. Soc. **96**(15), 4750–4752 (1974).
16. E. Podstawka, Y. Ozaki, and L. M. Proniewicz, "Part I: Surface-Enhanced Raman Spectroscopy Investigation of Amino Acids and Their Homodipeptides Adsorbed on Colloidal Silver," Appl. Spectrosc. **58**(5), 570–580 (2004).
17. A. L. Jenkins, R. A. Larsen, and T. B. Williams, "Characterization of amino acids using Raman spectroscopy," Spectrochim. Acta A Mol. Biomol. Spectrosc. **61**(7), 1585–1594 (2005).
18. J. Jehlička, A. Oren, and H. G. M. Edwards, "Raman spectra of osmotic solutes of halophiles," J. Raman Spectrosc. **43**(8), 1134–1140 (2012).
19. L. B. Faria, F. M. Almeida, O. Pilla, F. Rossi, J. M. Sasaki, F. E. A. Melo, J. Mendes Filho, and P. T. C. Freire, "Raman spectra of L-histidine hydrochloride monohydrate crystal," J. Raman Spectrosc. **35**(3), 242–248 (2004).
20. S. Kecel, A. E. Ozel, S. Akyuz, S. Celik, and G. Agaeva, "Conformational analysis and vibrational spectroscopic investigation of L-proline-tyrosine (L-Pro-Tyr) dipeptide," J. Mol. Struct. **993**(1-3), 349–356 (2011).
21. N. K. Budhavaram and J. R. Barone, "Quantifying amino acid and protein substitution using Raman spectroscopy," J. Raman Spectrosc. **42**(3), 355–362 (2011).
22. J. Bandekar, "Amide modes and protein conformation," Biochim. Biophys. Acta **1120**(2), 123–143 (1992).
23. H. S. Shafaat, B. S. Leigh, M. J. Tauber, and J. E. Kim, "Spectroscopic Comparison of Photogenerated Tryptophan Radicals in Azurin: Effects of Local Environment and Structure," J. Am. Chem. Soc. **132**(26), 9030–9039 (2010).
24. G. P. Sousa, P. T. C. Freire, J. Mendes Filho, F. E. A. Melo, and C. L. Lima, "Low-Temperature Raman Spectra of L-Histidine Crystals," Braz. J. Phys. **43**(3), 137–144 (2013).
25. N.-T. Yu, B. H. Jo, and D. C. O'Shea, "Laser Raman Scattering of Cobramine B, a Basic Protein from Cobra Venom," Arch. Biochem. Biophys. **156**(1), 71–76 (1973).
26. C. Hunte, "Specific protein-lipid interactions in membrane proteins," Biochem. Soc. Trans. **33**(5), 938–942 (2005).
27. A. G. Lee, "Lipid-protein interactions," Biochem. Soc. Trans. **39**(3), 761–766 (2011).
28. H. A. Sánchez, G. Mese, M. Srinivas, T. W. White, and V. K. Verselis, "Differentially altered Ca^{2+} regulation and Ca^{2+} permeability in Cx26 hemichannels formed by the A40V and G45E mutations that cause keratitis ichthyosis deafness syndrome," J. Gen. Physiol. **136**(1), 47–62 (2010).
29. T. Kwon, B. Roux, S. Jo, J. B. Klauda, A. L. Harris, and T. A. Bargiello, "Molecular dynamics simulations of the Cx26 hemichannel: insights into voltage-dependent loop-gating," Biophys. J. **102**(6), 1341–1351 (2012).
30. A. Ianoul, M. N. Boyden, and S. A. Asher, "Dependence of the Peptide Amide III Vibration on the Φ Dihedral Angle," J. Am. Chem. Soc. **123**(30), 7433–7434 (2001).
31. F. Zonta, G. Polles, G. Zanotti, and F. Mammano, "Permeation pathway of homomeric connexin 26 and connexin 30 channels investigated by molecular dynamics," J. Biomol. Struct. Dyn. **29**(5), 985–998 (2012).
32. F. Zonta, G. Polles, M. F. Sanasi, M. Bortolozzi, and F. Mammano, "The 3.5 ångström X-ray structure of the human connexin26 gap junction channel is unlikely that of a fully open channel," Cell Commun. Signal. **11**(1), 15 (2013), http://www.biosignaling.com/content/pdf/1478-811X-11-15.pdf.
33. D. L. Beahm and J. E. Hall, "Hemichannel and junctional properties of connexin 50," Biophys. J. **82**(4), 2016–2031 (2002).

1. Introduction

The human connexin 26 (hCx26) hemichannel is known for a complex, multi-facetted gating process. Several gate mechanisms have been identified in electrophysiological and biochemical studies; most notably, plug gate, loop gate, fast gate, and various chemical gates [1–3]. Conformational changes are expected in plug and loop gating. The plug gate is assumed to be a yet to be determined N-terminal interaction with the channel pore, whereas the loop gate process is thought to be controlled by the extracellular loops EL1 and EL2, linking the four transmembrane helices (TM1-4) (see Fig. 1 for a schematic representation of the protein). In addition, the gating process of hCx26 also contains a temperature-sensitive trigger component of yet unknown properties, changing the conductivity for small molecules from low to high upon exceeding a temperature of 23°C [4].

Although, structural details of hCx26 were probed experimentally by AFM [5], X-ray crystallography [6], and electron microscopy studies [7], the structural changes likely involved in the gating processes and the temperature-sensor activity of the hCx26 hemichannel have yet to be confirmed experimentally.

#207404 - $15.00 USD Received 28 Feb 2014; revised 5 May 2014; accepted 5 May 2014; published 6 Jun 2014

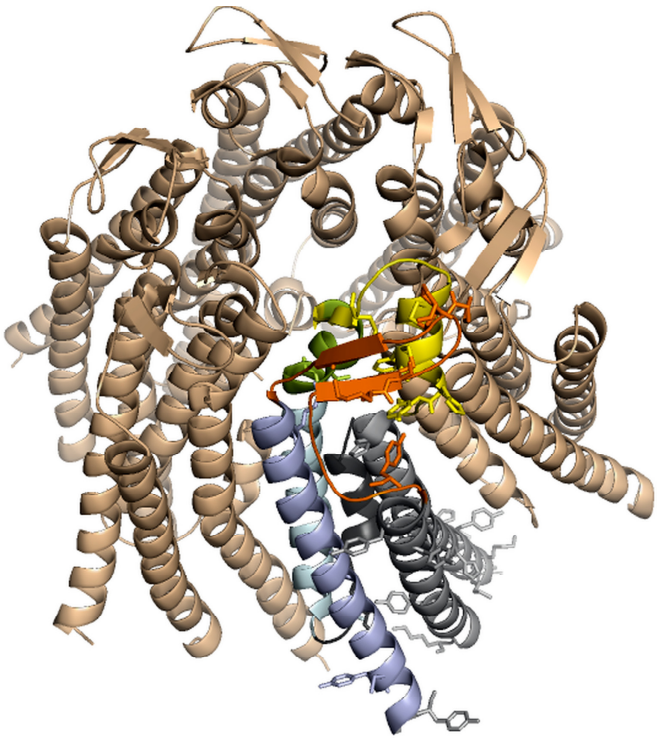

Fig. 1. Cartoon of the hCx26 channel showing six protomers. A single protomer is emphasized in color with the plug in dark grey, TM1 (cyan), TM2-3 (grey), TM4 (blue), EL1 (yellow), EL2 (orange), and the parahelix in green. (Structural data: pdb database (PDB ID: 2ZW3); edited with PyMol 1.6.0.0; PyMol Executable Build Copyright by Schrodinger, LCC).

Therefore, an in situ analysis of the functional protein, rather than its crystal or mutant, would be of great value for deepening our understanding of the hCx26 hemichannel. For this, Raman spectroscopy, providing information about the structure and dynamics of molecules, is one of the most promising techniques. UV resonance Raman scattering is used regularly to study protein conformations and their dynamics [8], but also conventional Raman spectroscopy in the visible range has been used successfully. For example, McColl et al. used Raman spectroscopic and Raman Optical Activity measurements at 514.5 nm excitation to monitor the α-helix to β-sheet transition of poly(L-lysine) as a function of temperature [9].

In this work, we used confocal Raman microscopy for the optical, non-invasive detection of structural differences in the hCx26 hemichannel at temperatures above and below the switching temperature of 23°C, for the first time. For this purpose, we recorded and analyzed high-precision Raman spectra of purified hCx26 at 10°C and 30°C in detergent with and without Ca^{2+} and lipid (POPC). The excitation wavelength of 532 nm is pre-resonant to the protic amino acids such as Tryptophan (Trp) and Lysine (Lys), thus allowing the recording of Raman spectra without favoring any of the protein constituents during the analysis.

The function and temperature susceptibility of the purified recombinant refolded hCx26 hemichannel was confirmed by electrophysiological analysis of the samples prior to the recording of the Raman spectra.

2. Experimental section

2.1 Chemicals and bacterial strains

POPC (1-palmitoyl-2-oleoyl-sn-glycero-3-phosphocholine) and DPPC (1,2-diphytanoyl-sn-glycero-3-phosphocholine) were obtained from Avanti Polar Lipids Inc. (Alabaster, Alabama, USA). IMAC cobalt-chelating resin (TALON) was purchased from Takara (Saint-Germain-

#207404 - $15.00 USD Received 28 Feb 2014; revised 5 May 2014; accepted 5 May 2014; published 6 Jun 2014

en-Laye, France), OG (n-octyl-β-D-glucopyranoside) from Glycon Biochemicals GmbH (Luckenwalde, Germany), and Topo cloning kits from Life Technologies GmbH (Darmstadt, Germany).

The *Escherichia coli* strains TOP10 and BL21plys (Life technologies GmbH, Darmstadt, Germany) were used to host the plasmid pTrcHisTopo containing the hCx26 gene. *E. coli* cells were cultivated in Luria Bertani medium (LB) using ampicillin as selection marker (100 μg ml^{-1}) at 37°C.

2.1 Synthesis of recombinant hCx26

The open reading frame encoding connexin hCx26 was expressed as described previously and purified by a cobalt-chelating resin with minor modifications [10]. *E. coli* lysates from 10-15 g cells were solubilized in 200 ml NLS-buffer, containing 55 mM N-laurylsarcosine, 200 mM NaCl, 50 mM NaHPO4, 1.09 M glycerin and 10 mM Tris pH 9.5, with added 20 μl protease inhibitor (P8849, Sigma-Aldrich), and centrifuged at 30000xg for 1 h.

The supernatant was diluted to a final detergent concentration of 0.5 per cent NLS and incubated with 7 ml IMAC resin at 4°C for 16 h. Unbound protein was removed by washing with 50 ml 0.5 per cent NLS, 200 mM NaCl, 10 mM Tris pH 8, and an additional washing step with 10 ml OG buffer, containing 30 mM OG, 200 mM NaCl, and 10 mM Tris pH 8 to change the detergent in the buffer to 30 mM OG.

The bound connexin hCx26 protein was eluted into 30 mM OG, 500 mM imidazole and 10 mM Tris pH 8. The buffer of the eluted fraction was diluted five-fold with 50 mM NaCl, 2 mM $CaCl_2$, and 20 mM Tris pH8 before being concentrated ten-fold by a YM 30K concentrator (Millipore) centrifuged at 3000xg followed by three dilution/concentration cycles.

The concentration of the protein was calculated based on the estimated absorption at 280 nm with an extinction coefficient of 53900 $M^{-1}cm^{-1}$ and adjusted to 1 mg ml^{-1}. Tag removal was performed in the presence of FaXa protease by incubating 40 U FaXa with purified 2 mg hCx26 over night at 23°C.

Digested hCx26 monomers were separated by anion exchange chromatography. The purified hCx26 protein was dialyzed overnight at room temperature in the presence of POPC at a protein:lipid ratio of 1:1 (w/w) against 100 mM NaCl and 10 mM Tris pH 8. The dialyzed batch was subsequently frozen in liquid nitrogen and stored at −80°C.

2.3 Single channel recording of purified hCx26

Bilayers containing hCx26 were formed and analyzed using the automated, temperature-controlled patch clamp platform Port-a-Patch by Nanion Technologies (Nanion Technologies, Munich, Germany). This setup uses microstructured borosilicate glass chips with a 2 μm aperture. Suspended planar lipid bilayers are formed by spreading giant unilamellar vesicles (GUVs) over the aperture. GUVs were prepared from DPPC (Avanti Polar Lipids, Alabaster, USA), and dissolved in chloroform (0.01 M and 0.001 M cholesterol) using the Vesicle Prep Pro system (Nanion Technologies, Munich, Germany).

A volume of 0.06 μl of purified hCx26 (0.75 mg ml^{-1}) was dissolved in buffer solution (0.01 M Tris pH 8.0, 0.1 M NaCl, 0.002 M $CaCl_2$, 0.7 μM POPC, and 0.03 M OG) and added to the external side of the bilayer to a volume of 10 μl containing 0.2 M KCl, 0.005 M EDTA, and 0.01 M HEPES-KOH pH 7.2. An EPC-10 patch-clamp amplifier (HEKA Elektronik, Lambrecht/Pfalz, Germany) with the PATCHMASTER software (HEKA Elektronik) was used for data acquisition. Single channel analysis was performed using Origin 6.0 (OriginLabs, Northampton, MA-01060, USA).

2.4 Raman spectroscopy

Samples for Raman analysis were mounted on an uncoated 1.2 mm deep indentation slide and sealed with a coverslip to avoid evaporation during measurement.

#207404 - $15.00 USD Received 28 Feb 2014; revised 5 May 2014; accepted 5 May 2014; published 6 Jun 2014

The sample temperature was set and maintained thermoelectrically throughout the measurement using a Peltier element in direct contact with the microscope slide. The Peltier element (QC-127-1.0-3.9M by Quick-Ohm Küpper & Co. GmbH, Wuppertal, Germany) was controlled and monitored using a Newport 3040 temperature controller (Newport Spectra-Physics GmbH, Darmstadt, Germany) with a thermistor sensor (10 kΩ; Vishay Electronic GmbH, Selb, Germany). In order to confirm the absence of a thermal gradient within the sample, an external thermometer (Technotherm 9500 by Testoterm KG, Lenzkirch, Germany) equipped with a NiCr-Ni sensor was kept in direct contact with the cover slip. Temperature accuracy was ± 0.1°C with a temperature stability of 0.3°C/h. Sample temperature was adjusted to the target temperature 1 h before the measurement and held constant throughout the measurement.

Raman spectroscopy was performed with a confocal Raman microscope (CRM200 by WITec GmbH, Ulm, Germany), equipped with a standard objective (Nikon CFI LU Plan, 50x, NA 0.55). A frequency-stabilized, frequency-doubled continuous-wave Nd:YAG laser at 531.9 nm was used for excitation. Slit width was 50 µm, realized by a multimode fiber connecting the Raman microscope and the spectrometer (UHTS 300 by WITec). Laser intensity was set to 36 mW. The loss within the optics prior sample contact was 30 per cent.

The grating used for high-precision measurements had 1800 lines per millimeter. Spectra were recorded with an electron multiplying charge-coupled device (emCCD) camera (Andor DU970N-BV-353), electrically cooled to −69°C. The spectral resolution of the system in this configuration was 1 cm^{-1} with a spectral accuracy of 1 cm^{-1}. Recorded spectra covered the range between 400 and 1500 rel. cm^{-1}. Integration time per spectrum in this configuration was 20 s, resulting in an average of 25000 counts for each of the dominant Raman lines in the spectrum.

For obtaining a first overview of the spectral features, determining the fingerprint area of the hCx26 spectrum, and the areas of change within the spectrum, the system was initially operated with a 600 lines per millimeter grating. The overview spectra recorded with this setup covered the range between −120 and 3500 rel. cm^{-1} with a spectral resolution of 5 cm^{-1}. Here, integration time per spectrum was 100 s, limited by detector saturation in the strong H_2O Raman bulk between 3000 and 3500 rel. cm^{-1}.

The Raman measurements were performed with purified hCx26 in 30 mM octylglucoside, 100 mM NaCl, and 10 mM Tris pH 8, with hCx26 in detergent-POPC buffer (30 mM octylglucoside, 100 mM NaCl, 10 mM Tris pH 8, and 1.28 mM POPC), and with hCx26 in Ca^{2+}-buffered POPC buffer (30 mM octylglucoside, 100 mM NaCl,10 mM Tris pH 8, 1.28 mM POPC, and 2 mM $CaCl_2$) always prepared consecutively from the same protein batch. The measurements were performed on two different batches over several days. Protein concentration in the measured samples was adjusted to 2 mg ml^{-1}.

Overview and high-precision spectra as defined above were recorded at 10°C and 30°C sample temperature from both batches after each preparation step.

2.5 Data extraction and analysis

Raman spectra used for analysis were averaged over 50 individual spectra using WITec ScanCTRL software (WITec) to minimize statistical noise components. The analysis of the averaged Raman spectra was done with commercial spectral analysis software (OPUS 5.5 by Bruker) as described previously [11].

The dark spectrum with an intensity of approx. 800 CCD counts per spectrum was subtracted from all data sets. The analysis of the Raman data was done in two steps: peak analysis for each spectrum, and differences between the respective spectrum and the spectra recorded under different conditions or under the same conditions on a different day. The peak analysis consisted of determining the position and intensity of the peak for each Raman line. Since measurements were performed at two temperatures (10°C and 30°C) and thermal expansion may well alter the amount of protein in the measurement volume, changes in the total intensity of the spectra were discarded by vector-normalizing the spectra prior

#207404 - $15.00 USD Received 28 Feb 2014; revised 5 May 2014; accepted 5 May 2014; published 6 Jun 2014

subtraction. Differences between two spectra were determined by subtracting the background-corrected, fully vector-normalized spectra. The resulting difference spectrum was subsequently subjected to a peak analysis. Only difference peaks exceeding the average height and width of the noise jitter by at least a factor of two were considered in the final evaluation.

3. Results

3.1. Temperature-dependent activity of purified hCx26 by single channel recording

The channel function of purified hCx26 protein in lipid bilayer membranes was examined electrophysiologically. Single channels were analyzed at 19°C and 28°C, revealing a single channel conductance of approx. 1.6 pA at 19°C and 14 pA at 28°C and confirming a temperature-dependent activity of the single channel (see Fig. 2).

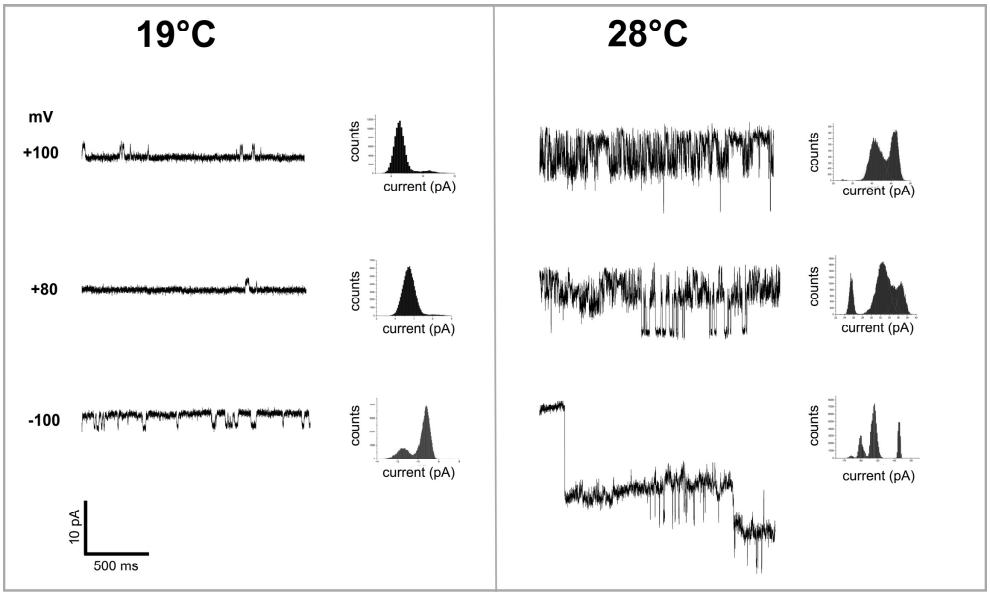

Fig. 2. Single channel recording (SCR) after functional reconstitution of hCx26 into a planar bilayer. Single channel traces at different applied voltages at 19°C and 28°C after leak subtraction and corresponding point-amplitude histograms.

3.2. Raman data

The four strongest features of the hCx26 Raman spectrum are in order of decreasing intensity: an intense double line at 1073 and 1060 rel. cm^{-1} with another band mounted on its higher wavenumber slope at 1122 rel. cm^{-1}, a second double line at 830 and 861 rel. cm^{-1}, a strong single peak at 1472 rel. cm^{-1}, and a narrow double line with peaks at 491 and 499 rel. cm^{-1}. Additional lines given in order of increasing wavenumbers are found at 425, 688, 933, 985, and two broad, overlapping bands centered at 1269 and 1313 rel. cm^{-1} (see Figs. 3 and 4).

For analyzing the structural changes in hCx26 due to conformational changes, Raman spectra for the various experimental conditions were compared by pairwise calculation of difference spectra, showing that one condition (hCx26 in Ca^{2+}-buffered POPC at 10°C) significantly deviates from all others.

The difference spectrum (30°C–10°C) covering the range between 400 and 1500 rel. cm^{-1} revealed six areas in which the Raman spectrum of hCx26 in Ca^{2+}-buffered POPC at 10°C differs from that at 30°C and at all other analyzed conditions (see Fig. 5). While the difference peaks at 501, 688, 930, and 1477 rel. cm^{-1} are comparatively moderate, the differences seen in the Raman bands at 861 and 1060 rel. cm^{-1} are more pronounced.

#207404 - $15.00 USD Received 28 Feb 2014; revised 5 May 2014; accepted 5 May 2014; published 6 Jun 2014

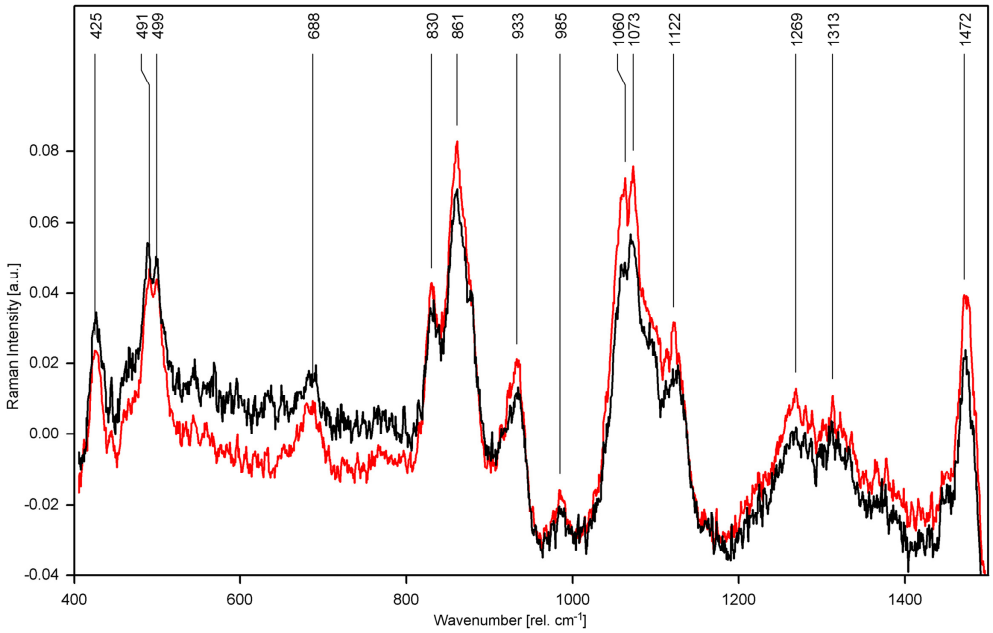

Fig. 3. Raman spectrum of purified hCx26 protein in Ca^{2+}-buffered POPC, recorded at 10°C (black) and 30°C (red). The average number of CCD counts per individual spectrum prior full-spectrum vector-normalization was 25000 counts (see Fig. 4 for the untreated spectra).

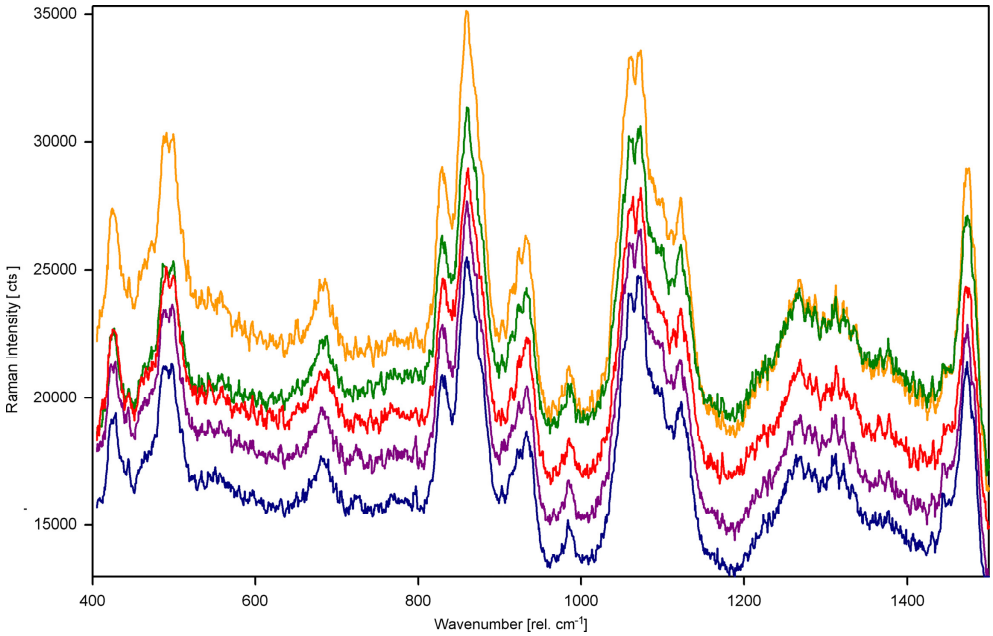

Fig. 4. Raman spectra as recorded of purified hCx26 in detergent buffer at 10°C (green) and 30°C (yellow), of hCx26 in POPC at 10°C (blue) and 30°C (purple), and hCx26 in Ca^{2+}-buffered POPC at 30°C (red). Note that these spectra differ solely by their total intensity. For an example of their spectral differences, see Fig. 5 (black spectrum).

#207404 - $15.00 USD Received 28 Feb 2014; revised 5 May 2014; accepted 5 May 2014; published 6 Jun 2014

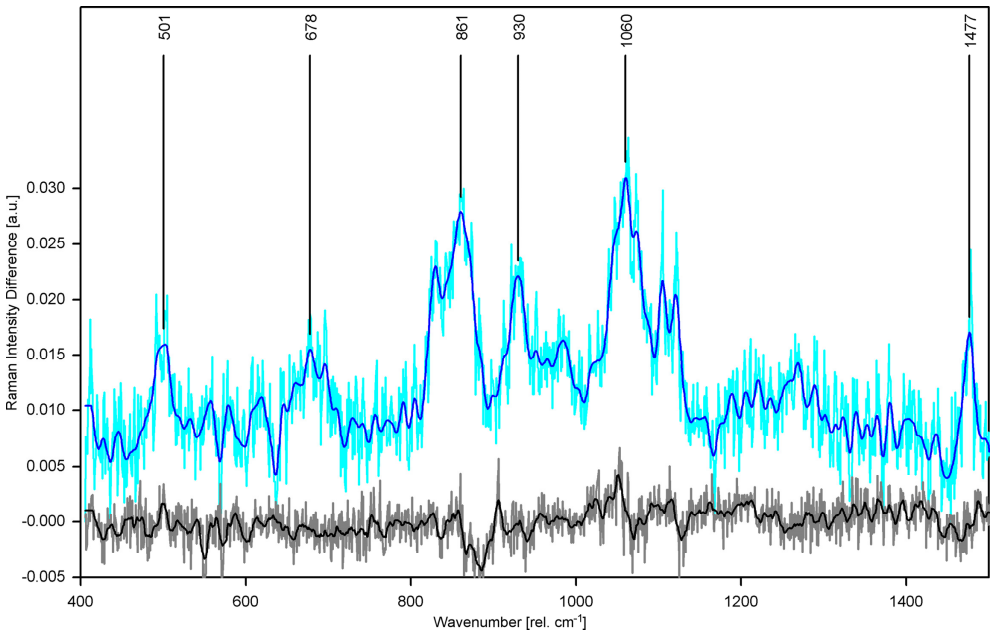

Fig. 5. Difference spectrum of purified hCx26 in POPC (black) and in Ca^{2+}-buffered POPC at 10°C and 30°C (blue). The difference spectra prior smoothing are given in grey and cyan, respectively. Raman spectra recorded at 10°C were subtracted from the respective spectra recorded at 30°C.

The overview spectra recorded from the first batch of protein are given as supplemental material. The Raman spectra, used to determine the fingerprint area and therein the area of the most notable changes in the spectra at different conditions, cover the range between −120 and 3000 rel. cm^1. The corresponding difference spectrum between 400 and 1500 rel. cm^{-1} is also included. Please note that the spectral resolution of the supplemental material (5 cm^{-1}) is significantly lower than the data presented here.

Neither the detergent buffer medium nor the POPC with and without Ca^{2+} show any Raman features exceeding the background in the protein Raman spectrum (data not shown).

4. Discussion

4.1 Raman spectrum of hCx26

The Raman spectrum of hCx26 recorded with 532 nm excitation is dominated by amino acids in an α-helical structure, in superposition with individual amino acids in various arrangements. See Fig. 3 for the annotated spectrum. A summary of the Raman bands and their tentative assignments including references is given in Table 1. A schematic of a hCx26 protomer with the Raman recognizable amino acids marked in color is given in Fig. 6.

The lack of intensity between 1235 and 1240 rel. cm^{-1} is a clear indicator of a primarily α-helical conformation of the protein with some small non-helical features [12–14]. This fits well with the known structure of the hCx26 protomer consisting of four trans-membrane αhelixes with short β-sheet structures in the extracellular loops [9] (see also Fig. 1). This is further supported by the peak at 933 rel. cm^1 ascribed to the C-C stretching vibration of the αhelical backbone [13], the shape of the Amide III region dominated by two broad, overlapping bands centered at 1265 and 1313 rel. cm^{-1}, and the characteristic CH deformation band at 1472 rel. cm^{-1} [15,16].

#207404 - $15.00 USD Received 28 Feb 2014; revised 5 May 2014; accepted 5 May 2014; published 6 Jun 2014

Table 1. Tentative assignment of Raman lines in the spectrum of hCx26

Raman band [rel. cm^{-1}]	tentative assignment	ref.
425	Pro (δ OCC)	[14,18]
491	His (δ R-N =)	[19,24]
499	Cys (ν SS)	[17]
688	AA Amide V (δ_{oop} NH)	[22]
830	Tyr (indole)	[17,25]
861	AA (ρ NH); Tyr (indole); Pro (pyrrole)	[12,17,25]
933	Pro & ν C-C (α-helix)	[13]
985	Tyr	[17]
1060	His (δ_{ip} C-H imidazole)	[19,24]
1073	AA (ν C-C, ν C-OH)	[14,18,20,21]
1122	AA (ν C-N)	[14,17,18]
1269	AA Amide III (α-helix)	[12,15,16]
1313	Pro & Lys (α-helix)	[12,15]
1472	Pro & Lys (δ CH α-helix)	[12,15,16]

δ: deformation; δ_{ip}: in-plane deformation; δ_{oop}: out-of-plane deformation; ρ: rocking; ν: stretching; AA: multiple amino acids and bonded amino acids; Cys: cysteine; His: histidine; Lys: lysine; Pro: proline; Tyr: tyrosine; R: unspecified remain.

Fig. 6. Cartoon of the hCx26 protomer with the amino acids identified in the Raman spectrum given in colored stick representation: cysteine (magenta), histidine (yellow), lysine (blue), proline (cyan), and tyrosine (orange). EL1, EL2, parahelix, and plug are darkened for easier orientation with respect to Fig. 1. (Structural data obtained from the pdb database (PDB ID: 2ZW3); edited by Open-Source PyMOL 1.6.0.0; PyMOL Executable Build Copyright by Schrodinger, LLC.)

The Raman band at 499 rel. cm^{-1} is caused by the disulfide bridges between cysteines (Cys) stabilizing the extracellular loops of the protomer [9,17], while the isolated Raman band at 425 rel. cm^{-1} is tentatively ascribed to proline (Pro). Additional bands reported for

#207404 - $15.00 USD Received 28 Feb 2014; revised 5 May 2014; accepted 5 May 2014; published 6 Jun 2014

protein-bound Pro are 863, 925, and 1075 rel. cm^{-1}, all of which overlap with strong bands originating from several amino acids or the α-helical backbone [14,18]. This conforms with the reported Pro-Cys-Pro motif seen in the extracellular loops of hCx26 [9], and is further supported by the high-wavenumber positions of the second Amide III band at 1313 rel. cm^{-1} and the CH deformation at 1472 rel. cm^{-1}, which point to a noticeable lysine (Lys) and Pro content of the α-helix [12,15,16].

The Raman bands at 830 and 861 rel. cm^{-1} consist of a known Fermi doublet caused by the indole ring of tyrosine (Tyr). In addition, the weak but distinct Raman band at 985 rel. cm^{-1} is also indicative of a strong Tyr component in the spectrum [17].

The higher wavenumber part of the Fermi doublet coincides with Raman bands originating from several amino acids, such as Lys (855), Pro (863), and Cys (866), resulting in the strong composite peak centered at 861 rather than 851 rel. cm^{-1} as it would be seen for pure Tyr [12,17]. The 872 rel. cm^{-1} band of Histidine (His) can be discerned on the high wavenumber shoulder of the 861 rel. cm^{-1} composite peak in the spectrum recorded in Ca^{2+}-buffered POPC at 10°C (Fig. 3), though it does not exceed the threshold for independent recognition. However, the presence of His is further validated by the Raman bands at 491 and 1060 rel. cm^{-1}, the latter of which Faria et al. tentatively identified as in-plane CH deformation of the imidazole group unique to His among protic amino acids [19]. While a component stemming from the thiol-group of Methionine (Met) in the band at 491 rel. cm^{-1} cannot be excluded, the notable lack of other Raman bands typically found in the Met and protic Met spectra point to a weak influence of Met on the Raman spectrum of hCx26 [16,17].

The high intensity of the asymmetrical peak at 1073 rel. cm^{-1}, associated with C-C and COH stretches, points to a strong influence of Pro (1075) and Cys (1085) on the spectrum [17,18,20,21]. The small peak at 1122 rel. cm^{-1} riding on the high wavenumber shoulder of the 1073 rel. cm^{-1} peak is tentatively assigned to the CN stretching [17,18].

The broadened Raman band centered at 688 rel. cm^{-1} is assigned to the Amide V mode, widely considered to be an NH out-of-plane motion with a CN torsion component [22].

Interesting in this context is the absence of the sharp, intense Raman band just above 1000 rel. cm^{-1} caused by the indole ring breathing in phenylalanine (Phe) and tryptophan (Trp), two amino acids known to be present in the external loops of hCx26 [9]. However, the results of Shafaat et al. showed this line to be severely reduced in protein-bound Trp radicals, pointing to similar effects acting on the other amino acids sporting indole groups under hydrophobic conditions [23].

4.2 Differences in the Raman spectrum of hCx26 recorded in Ca^{2+}-buffered POPC at 10°C

The strongest and most obvious difference of the Raman spectrum of hCx26 in Ca^{2+}-buffered POPC at 10°C to all other tested variations is the absence of the 1060 rel. cm^{-1} peak associated with the in-plane CH deformation of the imidazole ring unique to His among protic amino acids. It is noteworthy, that the Raman band at 491 rel. cm^{1}, associated with the skeletal structure of the His molecule [24], appears unaffected, indicating that it is indeed the imidazole group, protruding from the helix, which is affected (yellow in Fig. 6).

The Raman band at 861 rel. cm^{-1} loses intensity at 10°C, although it does not show a noticeable shift in the position of the composite peak. However, the related lower wavenumber band at 830 rel. cm^{-1} does not shift and even gains intensity in relation to the peak at 861 rel. cm^{-1}. This difference can be explained with a long known phenomenon related to the intensity ratio of the Tyr ring modes at 830 and 851 rel. cm^{-1} being sensitive to the environment of the Tyr side chain. A gain in intensity in the lower wavenumber mode indicates a loss of contact of the Tyr side chain with the environment. The original study of Yu et al. achieved this comparison by analyzing glycyl-tyrosine at room temperature and after heating to 85°C [25]. The heating to 85°C denatured the protein and thus exposed the tyrosine side chains, leading to the relative intensity of the two modes being reversed. Since the effect occurred in the cooled sample of hCx26 in Ca^{2+}-buffered POPC, we strongly assume a

#207404 - $15.00 USD Received 28 Feb 2014; revised 5 May 2014; accepted 5 May 2014; published 6 Jun 2014

conformational change burying Tyr side chains that are otherwise exposed to the environment in the incompletely closed channel.

In addition, the Raman lines associated with the disulfide bridges (499) and the Pro and Lys dominated CH deformation (1472) lose intensity on their high-wavenumber shoulder, resulting in the difference peaks at 501 and 1477 rel. cm^{-1}, respectively. While the Raman bands at 688 and 933 rel. cm^{-1}, associated with the Amide V region and the C-C stretching of the α-helical backbone respectively, display an equally moderate loss of intensity on their low wavenumber shoulders (difference peaks at 678 and 930 rel. cm^{-1}).

In contrast, the Amide III region with its broad bands centered at 1269 and 1313 rel. cm^{-1} is absent from the difference spectrum, as are the weak Raman lines at 425 (Pro), 491 (skeletal His), 985 (Tyr) and 1122 rel. cm^{-1} (CN stretching).

4.3 Implications for the hCx26 gating mechanism

Human Cx26 is thought to have annular lipids, linking the trans-membrane α-helices (TM1-4) with the bulk lipid bilayer. However, channel stabilization by non-annular lipids may also be an option, since hexamer formation occurs in the presence of POPC [26,27]. Given that the phase transition temperatures of the lipids used in the in vitro reconstitution of hCx26 are 41°C (DPPC) and 27-49°C (POPC) and thus above the experimentally determined temperature switch of 23°C in hCx26, it is possible that the protein-lipid interaction is limited below 23°C due to conformational changes in the protein itself. Mutations in the EL1 loop, like Gly45 or Ala40Cys, are known to affect the temperature sensitivity as well as the Ca^{2+}- and Cd^{2+}-sensitivity of hCx26 [3,28]. Considering that the identified Cys component in the Raman spectrum likely originates from the external loop Cys (Cys53, Cys60, and Cys64 on EL1) at a distance of 8, 15 and 19 amino acids from the supposed Ca^{2+}/Cd binding site, as well as from Cys169, Cys174 and Cys180 on the second external loop EL2, a moderately altered position of the EL1 loop at 10°C with respect to its position at 30°C may indeed be responsible for the slight loss of intensity on the high-wavenumber shoulder of the Raman band at 499 rel. cm^{-1}, associated with the disulfide bridges.

At 10°C in the presence of POPC lipid and Ca^{2+}, the hCx26 hemichannel is in its closed state, leading to a more compact protein structure, while at 28°C it is at least partially opened. The corresponding hCx26 Raman spectra indicate a decrease in exposed side chains of Tyr in the compact protein structure of the closed channel. As can be seen in Fig. 6 (orange), two groups of Tyr exist in the hemichannel: five Tyr are oriented to the external end of the hemichannel (Tyr65, Tyr68, Tyr152, Tyr155, and Tyr158), while five Tyr face the cytoplasmic end (Tyr102, Tyr103, Tyr105, Tyr108, Tyr125) (see Fig. 6, orange). Interestingly, the molecular dynamics model by Kwon et al. identified the loop gate of hCx26 as formed by the TM1/EL1 parahelix [29], consisting of the first trans-membrane α-helix TM1 and the first extracellular loop EL1. While the parahelix does contain two Tyr in EL1 (compare Figs. 1 and 6), altering the exposure of their side chains would require drastic conformational changes in the position of EL1 and 2. This does not fit with the merely moderate changes seen in the Raman line of the disulfide bridges (499 rel. cm^{-1}) and the Amide III region, most sensitive to peptide conformational changes [30], being absent from the difference spectrum (compare Fig. 5).

However, in the model of Kwon et al., loop movement depends on a complex net of interactions, notably involving Lys188 at the very beginning of TM4 [29]. An interaction of the EL1 loop with Lys188 may therefore extend the loop dynamic to TM4, thus affecting the position of the C-terminus and effectively bringing the three Tyr at the C-terminal end of TM4 into close contact with the bulk lipid, leading to the burial of their side chains in the closed state (10°C, POPC, and Ca^{2+}) of the hCx26 hemichannel. This may also explain the moderate changes seen in the Raman line at 933 rel. cm^{-1}, associated with the C-C stretching of the α-helical backbone, and in the Amide V mode at 688 rel. cm^{-1}.

#207404 - $15.00 USD Received 28 Feb 2014; revised 5 May 2014; accepted 5 May 2014; published 6 Jun 2014

These results are especially interesting with respect to the works of Zonta et al. [31,32], who analyzed calcein transport through hCx26, concluding that the solved X-ray structure by Maeda et al. [9] does not represent a fully opened hemichannel.

Especially noteworthy is a unique His component (1060) visible in the Raman spectrum of the open hCx26 channel, but absent in the spectrum of the fully closed channel. Electrophysiological experiments proved that His-modifying reagents like diethyl pyrocarbonate inactivate hemichannels, indicating an important role of His in the channel function [33]. Two His (His 67 and His74) exist in the EL1 loop, and additional His (His16, His94, His100) are oriented towards the internal side of the channel (see Fig. 6; yellow).

While a crystal structure of the fully closed hemichannel is not yet available, the crystal structure of the open hemichannel as known shows His67 as part of the EL1 loop and His16 as part of the plug domain in free position. Therefore, the existence of the Raman line at 1060 rel. cm^{-1} belonging to the imidazole group of His may directly indicate the open state of the channel (exposed His); whereas its absence signifies the closed state (covered His). This would imply that the fully closed state of hCx26 indeed involves the loop as well as the plug domain of the hemichannel.

5. Conclusions

The Raman spectrum of hCx26 was completely analyzed, accounting for all spectral features discernible between 400 and 1500 rel. cm^{-1}. Special attention was given to the differences seen in the spectrum of the fully closed channel achieved at 10°C in Ca^{2+}-buffered POPC.

Spectral components originating from specific amino acids (Tyr, His, Cys) and the α-helical backbone confirm that the TM1/EL1 parahelix and probably the TM4 trans-membrane helix are involved in the gating process responsible for fully closing the hemichannel.

The absence of the Raman line at 1060 rel. cm^{-1}, tentatively assigned to the imidazole group of Histidine, proved to be a direct indicator for the fully closed state of the hCx26 hemichannel. It may also indicate an additional involvement of the plug domain in the temperature-sensitive gating mechanism of hCx26.

To the best of our knowledge, this is the first analysis of purified hCx26 protein and protein function based on Raman spectroscopy. The results are in good agreement and partially confirm previous assumptions about the complex hCx26 gating process based on molecular dynamics, X-ray crystallography, and electrophysiology. High-precision Raman spectroscopy in the visible range proved to be a promising tool for the in situ analysis of proteins and their functional conditions.

Acknowledgments

We acknowledge support by Deutsche Forschungsgemeinschaft and Open Access Publishing Fund of Leibniz Universität Hannover.